Available online at www.sciencedirect.com
ScienceDirect
Journal of Solid State Chemistry 180 (2007) 2978–2985
JOURNAL OF SOLID STATE CHEMISTRY
www.elsevier.com/locate/jssc

Hematite template route to hollow-type silica spheres

Yang-Su Han[a], Gee-Young Jeong[a,b], Sun-Young Lee[a], Ho-Kun Kim[b,*]

[a]Nanomaterial Laboratory, Nanospace Co. Ltd., Ansan Digital Park #6032, 1123 Singgil-dong, Danwon-gu, Ansan, Gyunggi-do 425-839, Republic of Korea
[b]Department of Applied Chemistry, Hanyang University, Sa-1-dong, Sangnok-gu, Ansan 425-791, Republic of Korea

Received 12 June 2007; received in revised form 14 August 2007; accepted 15 August 2007
Available online 31 August 2007

Abstract

Hollow-type silica spheres with controlled cavity size were prepared from Fe_2O_3–SiO_2 core–shell composite particles by selective leaching of the iron oxide core materials using acidic solution. The spherical Fe_2O_3 core particles with a diameter range of 20–400 nm were first prepared by the hydrolysis reaction of iron salts. Next, the Fe_2O_3–SiO_2 core–shell particles were prepared by the deposition of a SiO_2 layer onto the surface of Fe_2O_3 particles using a two-step coating process, consisting of a primary coating with sodium silicate solution and a subsequent coating by controlled hydrolysis of tetraethoxysilicate (TEOS). The Fe_2O_3 core was then removed by dissolving with acidic solution, giving rise to hollow-type silica particles. Scanning electron microscopy clearly revealed that the cavity size was closely related to the initial size of the core Fe_2O_3 particle. According to the cross-sectional view obtained by transmission electron microscopy, the silica shell thickness was about 10 nm. The porous texture of the hollow-type silica particles was further characterized by nitrogen adsorption–desorption isotherm measurements.

Keywords: Hollow silica; Hematite; Core–shell particle; Acid washing; Nitrogen isotherm

1. Introduction

Hollow-type materials have attracted great attention in recent years because of their broad range of applications [1,2]. For example, they are used as delivery vehicles for the controlled release of substances such as drugs, cosmetic ingredients, dyes, and inks; for the protection of biologically active macromolecules [3–8]; as light-weight fillers [9]; as shape-selective adsorbents and catalysts [10–14]. As shown in recent studies, a variety of chemical and physico-chemical methods have been employed to produce hollow spheres composed of polymer, glass, and ceramic materials, including nozzle reactor approaches (spray drying and pyrolysis) [15–19], heterophase polymerization combined with a sol–gel methods [20–30], emulsion–interfacial polymerization strategies [31–41] and self-assembly processes [42–46].

In a typical procedure, template particle are coated in solution either by controlled surface precipitation of inorganic precursors (silica, titania, etc.) or by direct surface reactions that utilize specific functional groups on the cores to create core/shell composites. The template particles are subsequently removed by selective dissolution in an appropriate solvent or by calcinations at elevated temperatures in air to generate hollow spheres. In the sacrificial core template methods, the inorganic cores have been successfully employed as a structure-directing agent in obtaining nanometer-sized hollow spheres. Chen et al. [47] reported the preparation of porous hollow silica nanoparticles with a diameter of 60–70 nm and wall thickness of approximately 10 nm by using $CaCO_3$ nanoparticles as the inorganic template. Darbandi et al. [48] prepared porous silica nanoparticles with hole diameter of about 6.5 nm and wall thickness of 15 nm by using luminescent CdSe/ZnS cores as templates. Ammonia was used as catalyst for the polymerization of silica and to dissolve the CdSe/ZnS cores at once. Hao et al. [49] also reported the preparation method of an anisotropic silica hollow capsule from the Fe_2O_3–SiO_2–polypyrrole composite particle by selective removal of hematite cores.

For hollow-type silica, however, there is no systematic approach to controlling cavity size using inorganic core

*Corresponding author. Fax: +82 31 310 8533.
E-mail address: hkkim@hanyang.ac.kr (H.-K. Kim).

0022-4596/$ - see front matter © 2007 Elsevier Inc. All rights reserved.
doi:10.1016/j.jssc.2007.08.016

particles. Therefore, the development of a simple method to prepare hollow silica with controlled cavity size remains a great challenge to materials scientists. In this paper, a novel technique to fabricate hollow silica with different cavity sizes is described. An inorganic template is employed with shape-controlled iron oxide as a sacrificial core. In comparison with other techniques, the primary differences and advantages of this new process are: (a) monodisperse Fe_2O_3 particles with various particle morphology are prepared via controlled hydrolysis reaction to obtain morphogenic SiO_2 hollow silica and (b) the hydrolysis and condensation of silica is carried out by a two-step coating process to control the porous texture of the silica wall.

2. Experimental

2.1. Materials

Reagent-grade ferric chloride hexahydrate ($FeCl_3 \cdot 6H_2O$, 99%, Aldrich), ferric nitrate nonahydrate ($Fe(NO_3)_3 \cdot 9H_2O$, 98%, Aldrich), tetraethoxysilicate ($Si(OC_2H_5)_4$, (TEOS), 97%, Junsei), HCl, HNO_3, and NH_4OH (28%, Daejung Chem. Co.) were used as received without further purification.

2.2. Preparations

2.2.1. Preparation of hematite core particles

A schematic view of the synthetic process used is provided in Fig. 1. Spherical-type hematite core particles were prepared from the forced hydrolysis of acidic aqueous Fe(III) solution as described elsewhere [50]. In order to control the particle size, the molar fraction of coordinative Cl^- to non-coordinative NO_3^- ions to Fe(III) ions in the solution was systematically changed by varying the molar fraction of $FeCl_3$ to $Fe(NO_3)_3$. The total concentrations of Fe^{3+} and acid (H^+) in the reaction solution were fixed at 3.12×10^{-2} mol/dm^3 and 3.20×10^{-2} mol/dm^3, respectively. In the present study, the molar fraction of $FeCl_3$ (xFeCl$_3$, $x\mathrm{FeCl_3} = [\mathrm{FeCl_3}]/[\mathrm{FeCl_3} + \mathrm{Fe(NO_3)_3}]$) was controlled to 0.0, 0.2, 0.6, and 1.0, respectively. In order to obtain crystalline hematite particles with different particle sizes, the reaction mixtures were hydrolyzed and crystallized by refluxing at 100 °C for 7 days under continuous stirring. The reaction products were then separated by centrifugation and washed repeatedly with distilled water to remove all extraneous ions. Finally, crystalline hematite powders were obtained by drying the precipitates at 60 °C for 12 h.

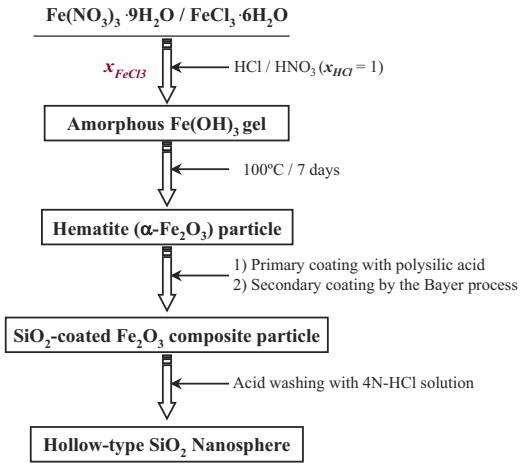

Fig. 1. Schematic diagram for the preparation of hollow-type silica particles.

2.2.2. Preparation of core–shell particles

For the monodisperse core–shell particles, a two-step coating based on the sol–gel process was used in this study. In the first step, the surface of core particles was coated with oligomeric silicate species using a polysilicic solution. The acidic polysilicic solution was prepared by the controlled hydrolysis of TEOS in the presence of an acid catalyst. In a typical preparation, 46 g of TEOS and 354 g of distilled water was mixed, and the solution pH was controlled to 4 by adding 1 N HCl solution. The solution was then continuously stirred for 12 h to obtain a transparent clear sol solution without phase segregation. In the coating process, one gram of the core particles obtained in the above was dispersed in 40 mL distilled water by ultrasonication for 20 min. Then, 1 mL of the polysilicic solution was added to the suspension at room temperature and mixed until homogeneous, with vigorous stirring for 30 min to deposit silicate species onto the surfaces of core particles. In addition, 1 mL NH_4OH was added to the suspension to facilitate hydrolysis of silicate, followed by further aging for 3 h at room temperature.

In the second step, the surface modified core particles were separated by centrifugation and re-dispersed homogeneously in 40 mL ethanol by ultrasonication. Then, 0.19 g of TEOS was added drop-wise to the ethanolic suspension, followed by the addition of 6 mL NH_4OH to achieve hydrolytic condensation of TEOS to SiO_2. The surface hydrolysis reaction was continued for 3 h at room temperature with continuous stirring. Finally, the coated particles were separated by centrifugation, washed with ethanol several times, and then dried at 60 °C for 12 h.

2.2.3. Preparation of hollow silica particles

The core–shell particles were then subjected to an acid leaching process to produce hollow-type silica particles. All the samples of core–shell type particles were dried at 100 °C for 2 h prior to the acid leaching experiment. In a typical leaching process, one gram of core–shell powder was added to 20 mL of a 4 N HCl solution, and the suspension was mechanically agitated for 2 h. During this process, the mother solution turned a reddish-brown color, indicating that ferric ions were leaching out. This process was repeated three times with centrifuging and refreshing the mother solution to completely remove the core materials.

Finally, the prepared hollow-type silica particles were washed with distilled water and dried at 60 °C for 12 h.

2.3. Characterization

Powder X-ray diffraction data were recorded at room temperature on a MAC Science MXP3A-HF22 using Cu$K\alpha$ radiation (40 kV, 30 mA). The apparent crystallite size was evaluated from the line-broadening of diffraction profiles using the Scherrer equation. The morphology and particle size of the samples were investigated by field emission scanning electron microscopy (FE-SEM, Hitachi S-4500) after the samples had been coated with Pt/Pd alloy for 180 s with an E-1030 ion sputter coater. Nitrogen adsorption–desorption isotherms were measured with a Micrometric ASAP-2010 using nitrogen at 77 K. Prior to the sorption measurements all the samples were degassed at 250 °C for 4 h under reduced pressure (<1 Torr). Specific surface areas were estimated using both BET and Langmuir equations. Micropore volumes (V_{micro}) and surface areas (S_{micro}) were also calculated based on the t-plot method of nitrogen. A t-curve for nonporous silica was used as a standard. Pore size distribution curves were calculated on the basis of the absorption branch of N_2 isotherms using the BJH method [51]. TEM observations were carried out using a JEOL JEM-200B microscope, with an accelerating voltage of 120 kV. The sample for TEM imaging was prepared by directly placing a drop of the aqueous dispersion of hollow particles on carbon-coated grids and letting the water evaporate slowly in air.

3. Results and discussion

3.1. X-ray diffraction

All of the particles that we prepared exhibited a characteristic XRD pattern of hematite (JCPDS 33-664) (Fig. 2). The dimensions of crystallite size for the four kinds of spherical hematite particles were also estimated from full width at half maximum (FWHM) of the powder XRD profiles with the Scherrer equation using the (012), (104) and (110) planes. The average crystallite sizes obtained are listed in Table 1 along with those of particle sizes observed by SEM. It can be seen in Table 1 that the average crystallite sizes prepared at $x\mathrm{FeCl_3} = 0.0$ and 0.2, 0.6 are 26.0, 48.0, and 64.8 nm, respectively, and are in close agreement with the particle sizes observed by SEM. The crystallite size prepared at $x\mathrm{FeCl_3}$ 1.0 is 27.5 nm, which is much smaller than that observed by SEM. This result implies that the particles produced at $x\mathrm{FeCl_3} \leqslant 0.6$ can be regarded as a single crystal, whereas those at $x\mathrm{FeCl_3} \geqslant 1.0$ are polycrystalline as previously reported [50].

3.2. Scanning electron microscopy

Spherical hematite particles were obtained from a forced hydrolysis reaction of acidic Fe(III) solution by changing

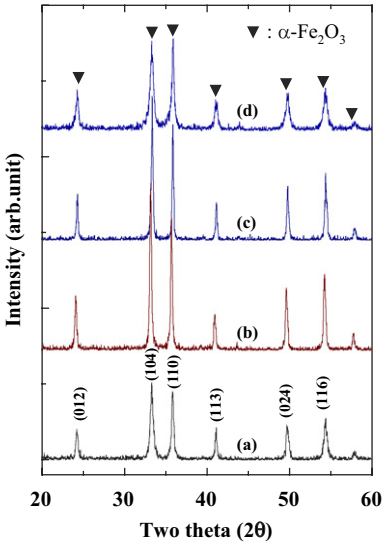

Fig. 2. Powder X-ray diffraction patterns of the hematite core particles with different $x\mathrm{FeCl_3}$ morphologies: (a) $x = 0.0$, (b) $x = 0.2$, (c) $x = 0.6$, and (d) $x = 1.0$.

the molar fraction of coordinative Cl^- to non-coordinative NO_3^- ions to Fe(III) ions in the solutions. Fig. 3 shows typical SEM micrographs of precipitated particles after aging for 7 days at various values of x. It is evident from Fig. 3 that the size of the spherical particles increased with an increase in $x\mathrm{FeCl_3}$, but did not change morphologically. The mean particle diameter measured from SEM pictures (Table 1) as a function of the molar fraction of $\mathrm{FeCl_3}$ ($x\mathrm{FeCl_3}$) increased from 25 to 400 nm with increasing $x\mathrm{FeCl_3}$. This result indicates a pronounced effect of Cl^- ions on particle size as described before [50]. The formation of large hematite particles from the forced hydrolysis reaction of an acidic Fe(III) aqueous solution was explained by the aggregation of the fine primary particles as confirmed by Scherrer calculation.

Fig. 4 presents SEM micrographs of the SiO_2 coated hematite core particles. It can be observed that the average particle sizes were slightly increased (Table 1), and the particle surfaces became smooth upon coating with silica layers. Fig. 5 shows the scanning electron microscopy images of the hollow microspheres after removal of core hematite particles by acid washing. It is worth noting that the spheres remained intact and preserved the three-dimensional spherical shape of particles even after removing the core materials. In the case of the smallest hollow particles (Fig. 5(a)), a partial collapse of spherical morphology and irregular coagulation between the particles is observed. This was probably caused by partial destruction of the SiO_2 shell during the acid leaching step, or by a partial breakage of the spheres during SEM measurement due to the vacuum in the SEM. The collapse of the spherical morphology may indicate that the silica wall thickness was not in all cases sufficient to maintain the initial spherical structure of the hollow SiO_2 particles. SEM

Table 1
Particle size and porous parameters of the core, core–shell and hollow particles with different core size

Sample ID		Particle size (nm)		Surface area (m^2/g)		Total pore volume, V_{total} (mL/g)	Average pore diameter (nm)[b]
Stage	xFeCl$_3$	XRD[a]	SEM	S_{BET}	S_{Lang}		
Core	0.0	26.0	~25	45.6	62.9	0.19	139.4
	0.2	48.0	~50	31.5	43.3	0.15	215.9
	0.6	64.8	~150	16.2	22.2	0.04	149.0
	1.0	27.5	~400	760.4	1055.3	0.89	59.3
Core–shell	0.0	–	~30	60.0	82.5	0.18	186.5
	0.2	–	~60	47.1	64.2	0.08	143.7
	0.6	–	~160	26.0	35.1	0.03	97.2
	1.0	–	~400	57.1	77.7	0.04	46.7
Hollow	0.0	–	~30	576.6	786.6	0.42	31.6
	0.2	–	~60	510.4	696.6	0.64	48.4
	0.6	–	~160	303.7	415.0	0.65	41.5
	1.0	–	~4000	447.5	616.5	0.75	85.7

[a]Calculated from the FWHM using the Scherrer equation.
[b]Calculated by the BJH method using desorption isotherm.

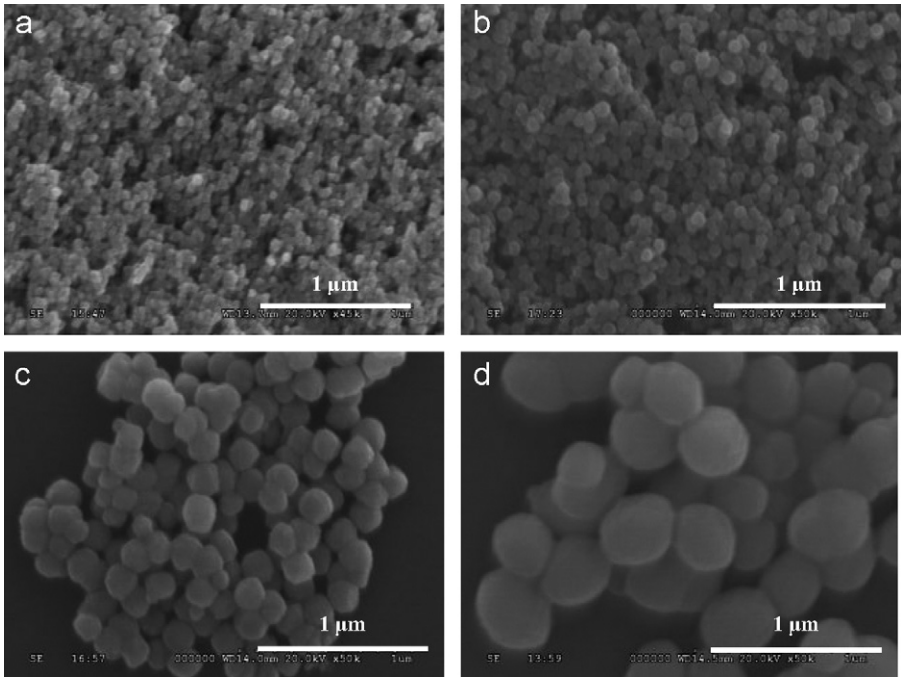

Fig. 3. Scanning electron micrographs of the core (α-Fe_2O_3) particles with different xFeCl$_3$: (a) $x = 0.0$, (b) $x = 0.2$, (c) $x = 0.6$, and (d) $x = 1.0$.

images of Fig. 5(b)–(d) clearly indicate the formation of discrete hollow-type silica particles with cavity sizes corresponding the hematite core particles, suggesting that the cavity size and morphology of hollow-type materials are easily tunable using a hematite core template with different particle size and morphology.

3.3. Transmission electron microscopy

Fig. 6 shows a representative TEM micrograph of the hollow particles obtained at xFeCl$_3 = 0.6$ with an average particle size of ~150 nm. The noticeable difference in contrast in the spheres after core removal confirms that hollow spheres were obtained upon acid leaching of the core matter. Wall thickness, as estimated by TEM from the ring around the perimeter of the hollow spheres, was approximately ~10 nm. TEM micrographs of hollow silica spheres show that the sphericity of the core Fe_2O_3 was preserved. No holes or traces of rupture are identified in this image, indicating that acid-leaching provided suitably mild conditions for core removal. Furthermore, in contrast to polymeric core particles, the inorganic template shows

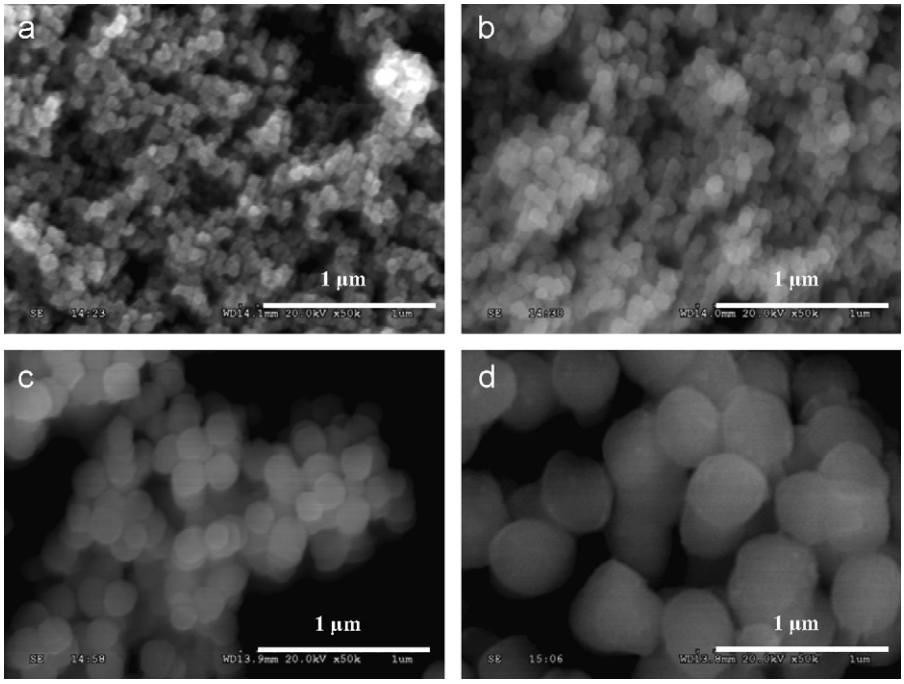

Fig. 4. Scanning electron micrographs of the core–shell (α-Fe_2O_3–SiO_2) particles with different $x$$FeCl_3$: (a) $x = 0.0$, (b) $x = 0.2$, (c) $x = 0.6$, and (d) $x = 1.0$.

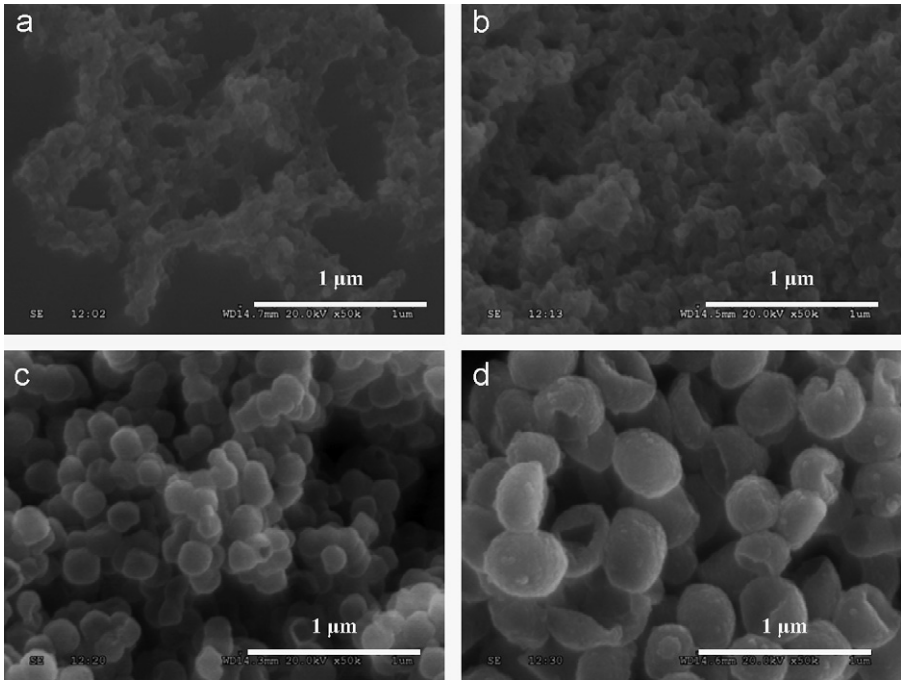

Fig. 5. Scanning electron micrographs of the hollow (SiO_2) particles with different $x$$FeCl_3$: (a) $x = 0.0$, (b) $x = 0.2$, (c) $x = 0.6$, and (d) $x = 1.0$.

that no substantial swelling occurred in solution, therefore avoiding wall rupture.

3.4. Nitrogen adsorption–desorption isotherm

In order to obtain porous parameters including specific surface area, pore volume, and pore size, nitrogen adsorption–desorption isotherms were measured using liquid nitrogen (77 K). Fig. 7 compares the isotherm curves for the core, core–shell, and hollow particles obtained at different $x$$FeCl_3$. Values of the specific surface area (according to the BET and the Langmuir methods), the average pore diameter (according to BJH method), total pore volume, and micropore surface area and pore volume calculated from these isotherms (according to the t-plot method) are listed in Table 1. The adsorption isotherms for

the core, and core–shell particles obtained at $x\mathrm{FeCl_3} = 0.0$, 0.2, and 0.6 (Fig. 7(a)–(c)) belong to type III in the IUPAC classification [52], indicating the non-porous or macroporous nature of hematite particles. The specific surface areas (S_{BET}) and total pore volumes (V_{total}) of these particles (Table 1) decreased with an increase in $x\mathrm{FeCl_3}$; that is, with an increase in crystallite size. This indicates that the surface areas and pores mainly originated from the interstices between the particles. Therefore, the surface areas and pore volumes decreased with increasing primary particle size. After coating with silica, the porous parameters increased slightly, which may be due to the newly developed pores between the silica particles. It is noted here that the surface area of the particles obtained at $x\mathrm{FeCl_3} = 1.0$ exhibited an extremely large value of 760.4 m^2/g even though the SEM particle size was the largest among the four samples. As noted in the XRD analysis, this sample consisted of an agglomerate of nanometer-sized primary particles with an average crystallite size of ~28 nm, suggesting the formation of a large number of small pores between the nanocrystals. This is also strongly supported by the strong uptake of N_2 in the lower P/Po region (Fig. 7(d)), where the main nitrogen adsorption occurred at the micropores. Interestingly, the surface area and pore volume of these particles were drastically reduced upon coating with silica layers (Fig. 7(d) and Table 1), and the isotherm type was also changed to type II, a typical isotherm pattern for the non-porous adsorbent. This indicates that the fine pores formed between the hematite core particles were infused with silica during coating process, leading to a collapse of porous structure.

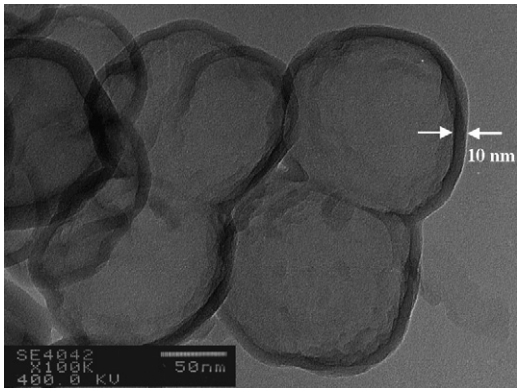

Fig. 6. Transmission electron micrograph of the spherical-type hollow silica particle with $x\mathrm{FeCl_3} = 0.6$.

As can be seen from Fig. 7 and Table 1, the surface areas and pore volumes of the hollow-type particles increased substantially compared with those of core–shell type particles, clearly suggesting the formation of porous materials after removal of the hematite core particles. The surface area was decreased as the molar fraction of $\mathrm{FeCl_3}$ ($x\mathrm{FeCl_3}$) was increased, that is, as the particle size

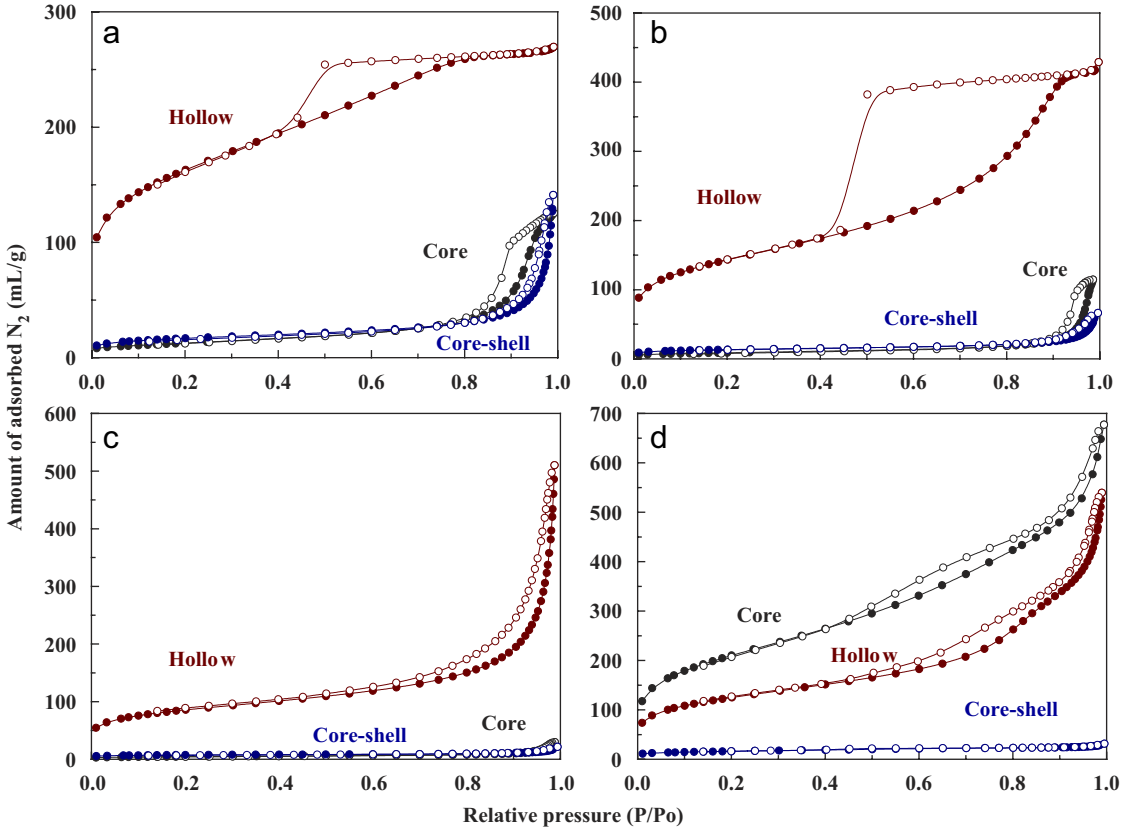

Fig. 7. Nitrogen adsorption–desorption isotherms of the core (α-Fe_2O_3), core–shell (α-Fe_2O_3–SiO_2) and hollow (SiO_2) type particles with different $x\mathrm{FeCl_3}$: (a) $x = 0.0$, (b) $x = 0.2$, (c) $x = 0.6$, and (d) $x = 1.0$.

was increased, except for the particles obtained at $x\mathrm{FeCl_3} = 1.0$. In the cases of $x\mathrm{FeCl_3} = 0.0$ (a) and $x\mathrm{FeCl_3} = 0.2$ (b), the isotherms can be classified as type IV according to the IUPAC classification [52], indicating the coexistence of micro- and mesopores with a distinct hysteresis loop.

The steep increase in nitrogen uptake at low P/Po domain strongly supports the presence of micropores with a pore size of <20 Å. Judging from the SEM and TEM observations, the pores developed after removing the core particles were mainly composed of mesopores with the size of 20–500 Å. Thus, it can be concluded that the newly developed micropores mainly originated from the silica walls, indicating that the silica shell was a porous layer. The large hysteresis loop between adsorption and desorption can be classified as type H2 hysteresis, according to IUPAC nomenclature [52]. In general, the hysteresis loop is closely related to the pore geometry, and the observed hysteresis shape was indicative of a corpuscular system like silica gels.

The adsorption–desorption isotherms of the $x\mathrm{FeCl_3} = 0.6$ (c) and $x\mathrm{FeCl_3} = 1.0$ (d) for the hollow-type particles can be classified as type II according to IUPAC nomenclature [52]. Type II describes adsorption on macroporous adsorbents with strong adsorbate–adsorbent interaction. Since the pore dimension in the hollow particles reflects the dimension of core particles, the large hematite core particles of size ~150 nm (c) and 400 nm (d) resulted in the large hollow cavities after removing the core materials. These large hollow cavities behave like macropores in the nitrogen adsorption–desorption isotherm. Along with the large N_2 sorption in the hollow cavities, a significant N_2 uptake at the lower P/Po region can be also observed, suggesting the presence of micropores, which can be assigned to the pores in the silica shell as previously mentioned. It is worth noting that the total pore volume (Table 1) of the hollow particles was proportional to the dimension of the core particles. This result provides further evidence that the volume occupied by core matter acted as a hollow cavity after removing the core species. As the core particle size increased, the total pore volume increased while the specific surface area decreased.

Pore size distribution curves for the hollow products are provided in Fig. 8. The distribution curves are calculated by the BJH method from the desorption branch. As shown in Fig. 8(a) and (b), the pore size distribution curves of the hollow particles obtained at $x\mathrm{FeCl_3} = 0.0$ and $x\mathrm{FeCl_3} = 0.2$ exhibited a narrow distribution, with values of ~30 and ~50 nm, respectively. This shows a good agreement with the expectation from the dimension of core particles. The distribution curve of the hollow particle obtained at $x\mathrm{FeCl_3} = 0.6$ (c) shows a broad pore size distribution with the average dimension of ~140 nm, corresponding to a core particle size of ~150 nm. The hollow sample prepared at $x\mathrm{FeCl_3} = 1.0$ (d) also displays a broad size distribution, reflecting the macropores formed after removal of the large core particles with an average size of ~400 nm. However, this sample also has a distribution maximum at around ~65 nm. Since the particles were aggregates consisting of ~30 nm primary particles, the inner surface of the silica shell had a porous nature with the shape of the primary crystals after removing the inorganic templates.

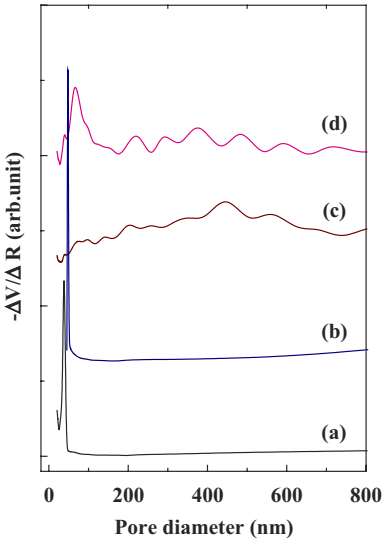

Fig. 8. Pore size distribution curves obtained from the desorption isotherm branches for the hollow-type particles with different $x\mathrm{FeCl_3}$: (a) $x = 0.0$, (b) $x = 0.2$, (c) $x = 0.6$, and (d) $x = 1.0$.

4. Conclusions

It has been demonstrated that the inorganic template route coupled with removal of the core using acidic solution provides a successful pathway for preparing inorganic hollow spheres in the nanometer to sub-micrometer size range. The important advantage of this method of fabricating hollow spheres is that the size and shape of the spheres obtained are determined by the dimensions of the hematite template employed. According to SEM and TEM observations, the core removal by acid washing resulted in the formation of hollow-type silica particles with the cavity size corresponding to that of hematite core particles and the thickness of silica shell was estimated to be ~10 nm. Nitrogen adsorption–desorption isotherm analysis revealed that the total pore volume is proportional to the size of core materials and the silica shell has a microporous structure.

References

[1] F. Caruso, Chem. Eur. J. 6 (2000) 413.
[2] G.B. Sukhorukov, A. Fery, M. Brumen, H. Möhwald, Phys. Chem. Chem. Phys. 6 (2004) 4078.
[3] F. Caruso, Adv. Mater. 13 (2001) 11.
[4] Z.Z. Li, L.X. Wen, L. Shao, J.F. Chen, J. Controlled Release 98 (2004) 245.
[5] J. Feng, M. Ruan, Y. Li, Angew. Chem. Int. Ed. 44 (2005) 5083.
[6] R.K. Sharma, S. Das, A. Maitra, J. Colloid Interface Sci. 284 (2005) 358.

[7] A.P.R. Johnston, C. Cortez, A.S. Angelatos, F. Caruso, Curr. Opin. Colloid Interface Sci. 11 (2006) 203.
[8] Y. Liu, H. Miyoshi, M. Nakamura, Colloid Surf. B: Biointerfaces 58 (2007) 180.
[9] D.L. Wilcox, M. Berg, Mater. Res. Soc. Symp. Proc. 372 (1995) 3.
[10] S.W. Kim, M. Kim, W.Y. Lee, T. Hyeon, J. Am. Chem. Soc. 124 (2002) 7642.
[11] G.S. Choi, S.B. Yoon, J.H. Kim, J.S. Yu, Chem. Commun. (2004) 2766.
[12] J.J. He, Y. Yoneyama, B.L. Xu, N. Nishiyama, N. Tsubaki, Langmuir 21 (2005) 1699.
[13] J.R. Song, L.X. Wen, J.F. Chen, Appl. Surf. Sci. 250 (2006) 2678.
[14] Y.H. Ng, S. Ikeda, T. Harada, T. Sakata, H. Mori, M. Matsumura, Adv. Mater. 19 (2007) 597.
[15] P.J. Bruinsma, A.Y. Kim, J. Liu, S. Baskaran, Chem. Mater. 9 (1997) 2507.
[16] Y. Lu, H. Fan, A. Stumo, T.L. Ward, T. Rieker, C.J. Brinker, Nature 398 (1999) 223.
[17] M. Iida, T. Sasaki, M. Watanabe, Chem. Mater. 10 (1998) 3780.
[18] P. Tartaj, T. González-Carreño, C.J. Serna, Adv. Mater. 15 (2003) 1620.
[19] K.D. Kim, K.Y. Choi, J.W. Yang, Colloid Surf. A: Physicochem. Eng. Aspect 254 (2005) 193.
[20] S. Schacht, Q. Huo, I.G. Voigt-Martin, G.D. Stucky, F. Schuth, Science 273 (1996) 768.
[21] F. Caruso, R.A. Caruso, H. Möhwald, Science 281 (1998) 495.
[22] D. Walsh, B. Lebeau, S. Mann, Adv. Mater. 11 (1999) 324.
[23] X.D. Wang, W.L. Yang, Y. Tang, Y.J. Wang, S.K. Fu, Z. Gao, Chem. Commun. (2000) 2161.
[24] K.H. Rhodes, S.A. Davis, F. Caruso, B. Zhang, S. Mann, Chem. Mater. 12 (2000) 2832.
[25] A. Imhof, Langmuir 17 (2001) 3579.
[26] D. Wang, R.A. Caruso, F. Caruso, Chem. Mater. 13 (2001) 364.
[27] W. Li, X. Sha, W. Dong, Z. Wang, Chem. Commun. (2002) 2434.
[28] I. Tissot, J.P. Reymond, F. Lefebure, E. Bourgeat-Lami, Chem. Mater. 14 (2002) 1325.
[29] H.J. Hah, J.S. Kim, B.J. Jeon, S.M. Koo, Y.E. Lee, Chem. Commun. (2003) 1717.
[30] Z. Dong, M. Chen, S. Zhou, B. You, L. Wu, Langmuir 22 (2006) 6403.
[31] K.B. Thurmond, T. Kowalewski, K.L. Wooley, J. Am. Chem. Soc. 119 (1997) 6656.
[32] J. Hotz, W. Meier, Langmuir 14 (1998) 1301.
[33] M. Okubo, Y. Konishi, H. Minami, Colloid. Polym. Sci. 276 (1998) 638.
[34] O. Emmerich, N. Hugenberg, M. Schmidt, S.S. Sheiko, F. Baumann, B. Deubzer, J. Weiss, J. Ebenhoch, Adv. Mater. 11 (1999) 1299.
[35] C.E. Fowler, D. Khushalani, S. Mann, J. Mater. Chem. 11 (2001) 1968.
[36] R.K. Rana, Y. Mastai, A. Gedanken, Adv. Mater. 14 (2002) 1414.
[37] W. Li, X. Sha, W. Dong, Z. Wang, Chem. Commun. (2002) 2434.
[38] T. Nakashima, N. Kimizuka, J. Am. Chem. Soc. 125 (2003) 6386.
[39] Q. Sun, P.J. Kooyman, J.G. Grossmann, P.H.H. Bomans, P.M. Frederik, P.C.M.M. Magusin, T.P.M. Beelen, R.A. van Santen, N.A.J.M. Sommerdijk, Adv. Mater. 15 (2003) 1097.
[40] Q. Sun, P.C.M.M. Magusin, B. Mezari, P. Panine, R.A. van Santen, N.A.J.M. Sommerdijk, J. Mater. Chem. 15 (2005) 256.
[41] B. Tan, H.-J. Lehroler, S.M. Vyes, B.L. Knutson, S.E. Rankin, Adv. Mater. 17 (2005) 2368.
[42] H. Zhao, L. Sun, R.M. Crooks, J. Am. Chem. Soc. 120 (1998) 4877.
[43] B.M. Discher, Y.Y. Won, D.S. Ege, J.C.H. Lee, F.S. Battes, D.E. Dsicher, D.A. Hammer, Science 284 (1999) 1143.
[44] M.S. Wendland, S.C. Zimmerman, J. Am. Chem. Soc. 121 (1999) 1389.
[45] S.P. Naik, A.S.T. Chiang, R.W. Thompson, F.C. Huang, Chem. Mater. 15 (2003) 787.
[46] R.K. Rana, V.S. Murthy, J. Yu, M.S. Wang, Adv. Mater. 17 (2005) 1145.
[47] J.F. Chen, H.M. Ding, J.X. Wang, L. Shao, Biomaterials 25 (2004) 723.
[48] M. Darbandi, R. Thomann, T. Nann, Chem. Mater. 19 (2007) 1700.
[49] L.Y. Hao, C.L. Zhu, W.Q. Jiang, C.N. Chen, Y. Hu, Z.Y. Chen, J. Mater. Chem. 14 (2004) 2929.
[50] K. Kandori, J. Sakai, T. Ishikawa, Phys. Chem. Chem. Phys. 2 (2000) 3293–3299.
[51] E.P. Barrett, L.G. Joyner, P.P. Halenda, J. Am. Chem. Soc. 73 (1951) 373.
[52] S.J. Gregg, K.S. Wsing, Adsorption, Surface Area and Porosity, second ed., Academic Press, London, 1982.